17th World Conference on Earthquake Engineering, 17WCEE
Sendai, Japan - September 13th to 18th 2020

DEVELOPMENT OF DESIGN GROUND MOTIONS INCORPORATING NEAR-FAULT EFFECTS

J. Lee[1], P. Kumar[2], B. Albin[3], Ibrahim Almufti[4], and K. Ellison[5]
[1] *Senior Engineer, Arup; currently Technical Principal, Mott MacDonald, jongwon.lee@mottmac.com*
[2] *Senior Engineer, Arup, pawan.kumar@arup.com*
[3] *Engineer, Arup, brian.albin@arup.com*
[4] *Associate Principal, Arup, ibrahim.almufti@arup.com*
[5] *Associate, Arup, kirk.ellison@arup.com*

Abstract

Forward directivity effects are often observed in strong ground motions recorded near causative fault(s) with the salient feature of a two-sided velocity pulse. The velocity pulse tends to be long-period (> about 1 sec) and generally has a large amplitude. Hence, the forward directivity effects are considered significant in designing long-period structures (e.g., tall buildings and base-isolated structures) situated in a region near active faults. Over the past decade, access to increased strong ground motion data and multiple studies have facilitated a better understanding of directivity effects and development of theoretical and/or empirical models that can be employed in engineering practice. Furthermore, with a growing emphasis on performance-based design, engineers have attempted to incorporate forward directivity effects in design ground motions where applicable. However, only a few of them have explicitly incorporated directivity effects in a probabilistic framework. This paper introduces a case history of design ground motions for a high-rise in downtown San Francisco, California, for which a probabilistic approach was used for incorporating directivity effects (velocity pulses). The probabilistic framework by Shahi and Baker (2011) was implemented in an in-house probabilistic seismic hazard analysis (PSHA) program, SISMIC, and used to account for near-fault effects and evaluate the site-specific characteristics of near-fault pulselike ground motions (e.g., pulse amplitude and pulse period) and their hazards. Also, the methodology per Almufti et al. (2015) was employed for developing suites of near-fault ground motions including pulselike motions based on the PSHA results. The design ground motions including the near-fault effects were developed in accordance with the design standard, ASCE 7-16. This methodology has been successfully used on past high-profile projects in San Francisco for nonlinear response history analyses such as seismic site response analysis and soil-structure-interaction analysis, subjected to rigorous peer review.

Keywords: near-fault effects, forward directivity, velocity pulse, ground motion, design ground motions, conditional mean spectra

1. Introduction

This paper presents a case history of developing design ground motions incorporating forward directivity effects for a new tall building (approximately 250-meters and 62 stories high) in downtown San Francisco, California, United States. The fundamental period (first mode) of the building in the two orthogonal directions is approximately 7.3 and 5.6 seconds. The project site is located approximately 14 km from the San Andreas fault and 16 km from the Hayward fault (see Fig. 1). Forward directivity effects are often observed in strong ground motions recorded near causative fault(s) with the salient feature of a two-sided velocity pulse. The velocity pulse tends to be long-period (greater than 1 sec) and generally has a large amplitude. Hence, the forward directivity effects are considered significant in designing long-period structures. Over the past decade, access to increased strong ground motion data and multiple studies have facilitated a better understanding of directivity effects and development of theoretical and/or empirical models that can be employed in engineering practice. Furthermore, with a growing emphasis on performance-based design, engineers have attempted to incorporate forward directivity effects in design ground motions where applicable. However, only a few of them have explicitly incorporated directivity effects in a probabilistic framework. This case study carried out probabilistic seismic hazard analyses (PSHA) incorporating near-fault effects in addition to conventional PSHA and evaluated the site-specific characteristics of near-fault pulselike ground motions and their hazards. Suites of near-fault ground motions including pulselike motions were developed based on the PSHA results. This methodology has been successfully used on past high-profile projects in San Francisco including the Salesforce, 181 Fremont, and Park Towers. The design ground motions including the forward directivity effects were developed in accordance with the design standard, ASCE 7-16 [1], and used for nonlinear response history analyses such as seismic site response analysis and soil-structure-interaction (SSI) analysis, subjected to rigorous peer review. The subsequent sections provide the procedure to develop bedrock-level design ground motions including forward directivity effects for site response and/or SSI analysis.

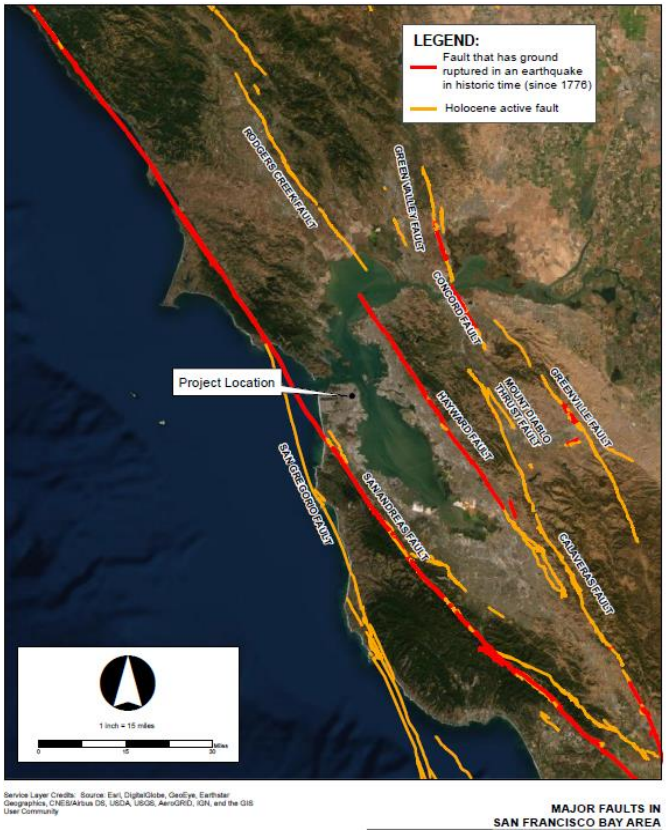

Fig. 1 – Site location and major faults around San Francisco

2. Seismic Hazard Assessment

A site-specific seismic hazard assessment was carried out performing both probabilistic and deterministic seismic hazard analyses in accordance with ASCE 7-16. A software for probabilistic seismic hazard analysis, nshmp [2], was used to determine site-specific probabilistic response spectra and seismic hazard information.

2.1 Seismic source and ground motion models

All known local and regional seismic faults significant to the project site in terms of ground shaking hazard have been identified and characterized as input in the probabilistic seismic hazard model. The same seismic source model as the 2014 National Seismic Hazard Map [3] was employed, which adopts the Uniform California Earthquake Rupture Forecast, Version 3 (UCERF3; [4]) for California.

A ground-motion model (GMM; attenuation relationship or ground motion prediction equation) relates the amplitudes of peak acceleration and response spectral acceleration to earthquake magnitude, source-to-site distance, site condition, and other causative parameters. All of the seismic sources considered in this study are shallow crustal faults. Hence, the GMMs used for this study are the Next Generation of Attenuation Models for the western United States (NGA-West2), including the following GMMs for estimation of horizontal ground motion [5 through 8]: Boore, Stewart, Seyhan, and Atkinson (2014); Campbell and Bozorgnia (2014); Chiou and Youngs (2014); and Abrahamson, Silva, and Kamai (2014). These GMMs were equally weighted in both probabilistic and deterministic hazard analyses. The selected NGA models use V_{S30} (travel time-averaged shear wave velocity in the upper 30 meters) as a measure to incorporate the effect of subsurface ground conditions on the site response. The site-specific V_{S30} value of 1,220 m/s was used for the bedrock, based on V_S measurements from downhole PS suspension logging performed at the site. The NGA-West2 GMMs result in rotation-independent, period-dependent 50th percentile (median) spectral accelerations, Sa_{RotD50} [9], simply denoted by RotD50. ASCE7 requires the Maximum Demand or RotD100 (rotation-independent, period-dependent 100th percentile; maximum) response spectra in developing design response spectra. Therefore, the RotD100 response spectra were determined by multiplying the RotD50 values by Maximum Demand factors (or RotD100/RotD50) per [10].

2.2 Hazard deaggregation

The seismic hazard disaggregation for spectral acceleration at relevant periods was obtained from the nshmp tool [2]. Table 1 summarizes the bedrock disaggregation results from the three sources with the largest contribution for the spectral periods, T = 0.75 and 7.5 sec, with the latter approximately representing the longer of the fundamental modes of the Tower (7.3 sec). The deaggregation results indicate that the hazard is governed by a M_W 8.0 event on the San Andreas fault (see Fig. 1), with a distance of R = 14.7 km, with minor contribution from the San Gregorio and Hayward faults. The hazard contribution from these three sources accounts for nearly 90% of the total seismic hazard. The deaggregation results are similar for T = 0.75 sec, which is representative of the higher mode response of the building.

Table 1 - Summary of deaggregation for T = 0.75 and 7.5 sec at bedrock from nshmp tool [2]

Period (sec)	Fault System	Distance (km)	Magnitude (M_W)	Hazard Contribution (%)
0.75	San Andreas	14.7	7.91	52.7
	San Gregorio	16.5	7.32	18.4
	Hayward	19.1	7.73	7.9
7.5	San Andreas	14.7	7.99	68.0
	San Gregorio	19.1	7.79	10.3
	Hayward	16.5	7.47	9.3

3. Site-specific Code-compliant Response Spectra at Bedrock

This section summarizes the development of site-specific acceleration response spectra at bedrock in accordance with ASCE 7-16. Note that all response spectra presented herein correspond to 5% damping.

The code-compliant (risk-targeted) Maximum Considered Earthquake (MCE_R) level spectra developed at bedrock was the basis for bedrock ground motion development. The MCE_R level spectrum is defined as the lesser of the probabilistic and deterministic spectral response accelerations in accordance with Section 21.2 of ASCE 7-16 where:

1. **Probabilistic**: the spectral response acceleration in the direction of *maximum* horizontal response from a 5% damped acceleration response spectrum associated with 2% probability of exceedance in a 50-year period, multiplied by a risk coefficient, C_R.
2. **Deterministic**: the deterministic spectral response acceleration from the 84th percentile, 5% damped spectral response acceleration in the direction of *maximum* horizontal response, but not less than the deterministic lower limit (LL) for Site Class B. The deterministic response spectra are generated by using the NGA-West2 GMMs with the controlling scenario defined as a M_w = 8.0 strike-slip event on the San Andreas fault at a source-to-site distance of 14.7 km, based on the hazard deaggregation at bedrock.

The Design Earthquake (DE) level response spectra are 2/3 of the MCE_R level spectra and shall not be less than 80% of the spectrum determined in accordance with Section 11.4.6 of ASCE 7-16. The resulting MCE_R spectrum at bedrock is shown in Fig. 2 along with the considered response spectra per code.

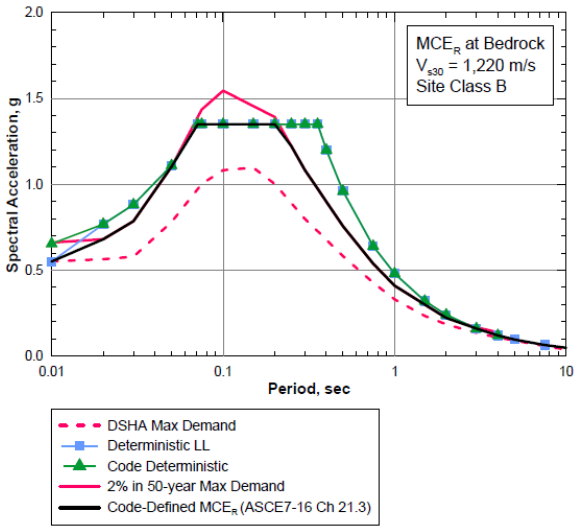

Fig. 2 – Code-compliant MCE_R at bedrock

4. Development of Horizontal Bedrock Target Response Spectra

This section summarizes the development of target response spectra at bedrock using the conditional mean spectrum (CMS) approach, and the selection and modification of bedrock time histories to be compatible with the target spectra.

4.1 Conditional Mean Spectra (CMS) at Bedrock

In recognition that the maximum spectral amplitudes at short and long periods do not occur in the same earthquake event and the characteristics of such earthquakes may be significantly different (pulselike or non-pulselike), a Conditional Mean Spectrum (CMS) approach [11, 12] was employed to characterize the short period and long period ground motions separately. Hence, two CMS suites were developed, which cover the code-defined period range of interest (0.4 – 10 sec). These are conditioned at the two periods: T = 0.75 sec (referred to as the "short period" suite, covering structural periods from 0.4 to 4 sec; and T = 7.0 sec (referred to as the "long period" suite, covering structural periods from 4 to 10 sec). For each of the two suites, the CMS is scaled such that the spectral ordinate at the conditioning period matches the code-defined MCE_R value at bedrock.

The short period CMS conditioned at T = 0.75 sec is scaled such that the spectral ordinate at T = 0.75 sec matches the code-defined MCE_R value at bedrock (0.53 g). At T = 0.75 sec, the controlling scenario for the 2,475-year hazard is a M_w8.0 event on the San Andreas fault at a source-to-site distance of 14.7 km. The deterministic (scenario) response spectrum was generated using the NGA-West2 GMMs and scaled to match the code MCE_R spectral acceleration at the conditioning period, T = 0.75 sec, followed by application of epsilon correlations between spectral accelerations at different periods per [12] to obtain the CMS. Since it is scaled to the MCE_R spectrum, this is referred to as the maximum demand CMS. The long period CMS conditioned at T = 7.0 sec is also scaled such that the spectral ordinate at T = 7.0 sec matches the code-defined MCE_R value at bedrock (0.07 g). The CMS was developed following the same procedure as the short period CMS. The resulting short period and long period CMS are shown in Fig. 3 along with the MCE_R, scenario response spectra, and max demand/RotD50 CMS.

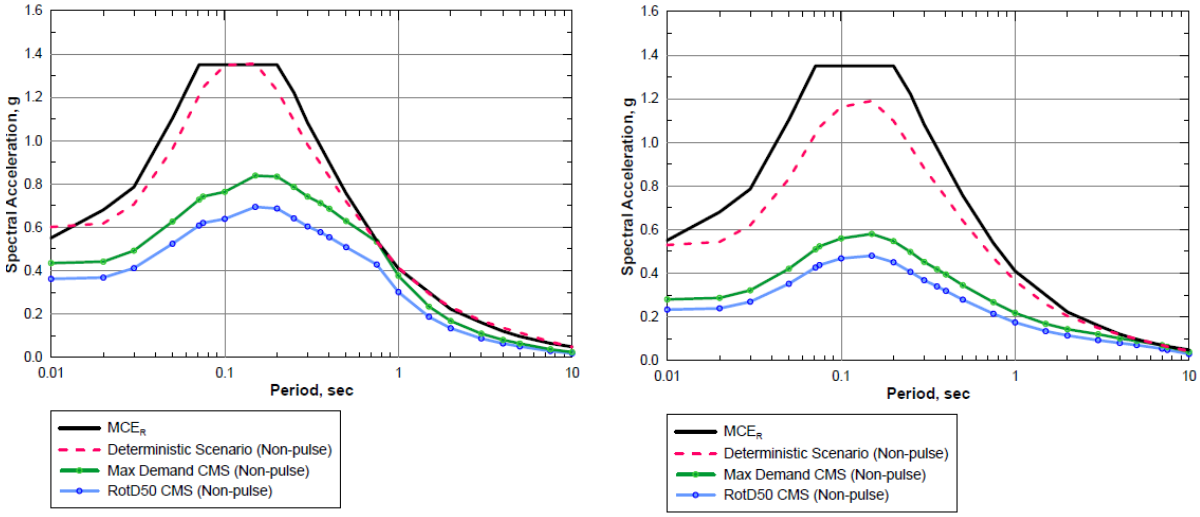

Fig. 3 – Short period (left) and long period (right) max demand and RotD50 CMS at bedrock; also shown are MCE_R and associated scenario response spectra.

4.2 Near-fault forward directivity pulses

Since the site is approximately 14 km from the San Andreas fault, the hazard is expected to be strongly influenced by the presence of near-fault forward directivity pulses that may govern the long period structural response. Pulselike motions amplify the response spectral acceleration of structures with periods above approximately 1 sec. The approach adopted to explicitly include the effect of near-fault directivity by incorporating velocity pulses in the design ground motions is described below.

4.2.1 Methodology for pulse-included seismic hazard at bedrock

This study employed the methodology per [13] using the probabilistic framework by [14, 15] to account for near-fault directivity effects, which extends the conventional PSHA model and incorporates additional parameters:

- Probability of a pulse given a site geometry based on [15].
- Probability of period of pulse (T_p) given an earthquake magnitude.
- Amplification of the spectral acceleration from a RotD50 GMM given a pulse occurs at a specific pulse period [15].
- Corresponding standard deviations on the pulse period and amplification terms; note that the period-dependent reduction of standard deviations for spectral accelerations of pulselike motions was disregarded, which was based on NGA-West1 data [14]. The reduction was not considered because practically no reduction in standard deviation for pulselike motions was observed from the NGA-West2 model [15].

The probabilistic approach per [14] was implemented in our in-house PSHA software SISMIC [16].

4.2.2 Pulse-included seismic hazard at bedrock

For both the short and long period suite CMS cases, the return period of the pulse-included Maximum Demand hazard was back-calculated corresponding to the MCE_R spectral acceleration, listed below:

- Short period: MCE_R = 0.53 g @ T = 0.75 sec – 1,700-year return period
- Long period: MCE_R = 0.07 g @ T = 7.0 sec – 760-year return period

The pulse-included uniform hazard response spectra (UHRS) for the short and long period suites are shown in Fig. 4. Hazard deaggregation analyses were performed for the 1,700-year and 760-year pulse-included uniform hazard for T = 0.75 sec and 7.0 sec, respectively. The hazard deaggregation indicated M_w 7.75 to M_w 8.25 events control the hazard for both the T = 0.75 sec and 7.0 sec. Also, the hazard is governed by pulselike motions. As shown in Fig. 5, the probability of a pulselike motion being observed at the site is approximately 59% and 76% for T = 0.75 sec and 7.0 sec, respectively. Fig. 6 shows the hazard contribution from pulselike motions with a broad range of pulse periods (T_p) for T = 0.75 sec and T = 7.0 sec. The remaining contribution to the hazard (from non-pulselike motions) is equal to 41% for T = 0.75 sec and 24% for T = 7.0 sec.

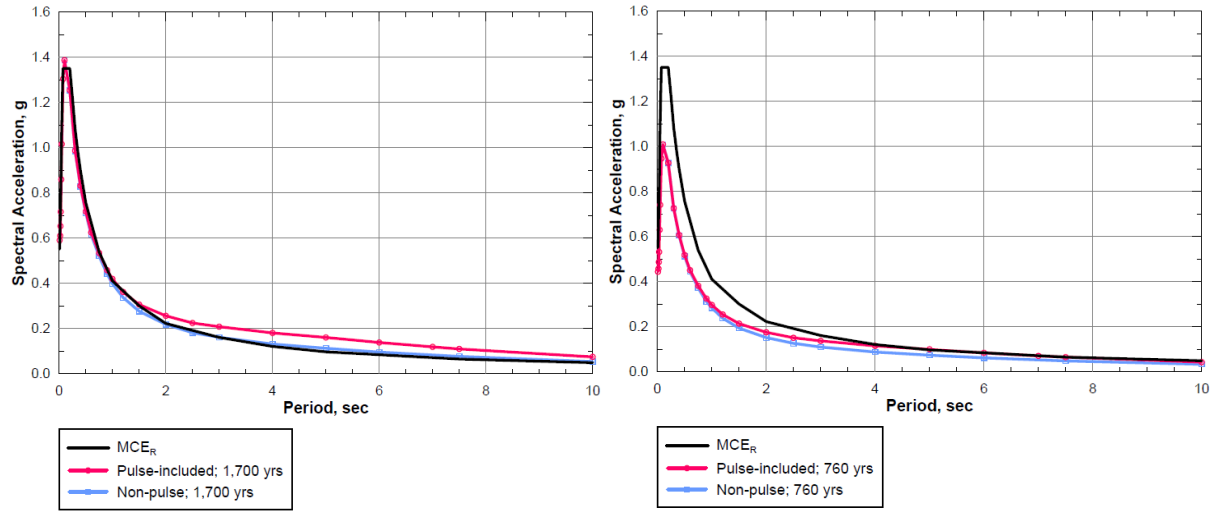

Fig. 4 – 1,700-year conventional UHRS and pulse-included UHRS versus MCE_R for T=0.75sec (left) and 760- year conventional UHRS and pulse-included UHRS versus MCE_R for T=7.0sec (right) at bedrock

4.3 Number of Ground Motions

ASCE 7-16 requires a total of eleven ground motions for each suite considered for nonlinear response history analysis. Therefore, a total of 22 sets of ground motions were developed, eleven each for the short and long period suites. Within each suite, the number of pulselike and non-pulselike motions was determined based on the pulse probabilities as a proportion of the total of eleven motions. The hazard contribution in terms of pulse period (Fig. 6) was used for calculating the normalized cumulative distribution as shown in Fig. 7. For both the CMS suites, the pulse period range was discretized into bins of equal hazard contribution, with the number of bins determined by the pulse probability for the respective suite. For the short period suite, with a pulse probability of 59% for T =0.75 sec, the T_p was discretized into six equal bins, whereas for the long period suite, with a pulse probability of 76% for T =7.0 sec, the T_p was discretized into eight equal bins (Fig. 7). The eight equally-weighted bins, which are defined as equal increments of the normalized cumulative distribution (six bins of 0.167 for short period and eight bins of 0.125 for long period). For example, the first bin in the long period suite would be defined by T_p between 0 and 3.70 sec (which is where 0.125 cumulative distribution intercepts the cumulative distribution curve). The second bin would be defined by T_p between 3.70 and 4.74 sec, and so on. Accordingly, six of the eleven motions were allocated in the short period suite to be pulselike. Similarly, for the long period suite, a total of eight pulselike motions were initially allocated.

However, during the peer review process, the first of the long period T_p bins was dropped and replaced by a relatively long duration non-pulselike motion for the following reasons:

1. Pulselike motions tend to be short-duration by definition, as they impart most of the energy over a short time period. Having the majority of ground motions being pulselike can lead to underestimation of the strong motion duration.
2. Having sufficiently long duration is particularly important for the long period suite, as the significant duration of the motions will dictate the number of cycles of strong motion, which will be fewer for longer structural periods.
3. The first long period T_p bin covers pulse period range that is also covered in the short period suite, which will govern the short period response of the building. Therefore, it is deemed less consequential to remove one shorter pulse period motion from the long period suite compared to having an excess of shorter duration motions.

Hence, the total number of bedrock motions is summarized as follows:

- Short Period (T = 0.75 sec): 11 motions – 6 pulselike and 5 non-pulselike
- Long Period (T = 7.0 sec): 11 motions – 7 pulselike and 4 non-pulselike

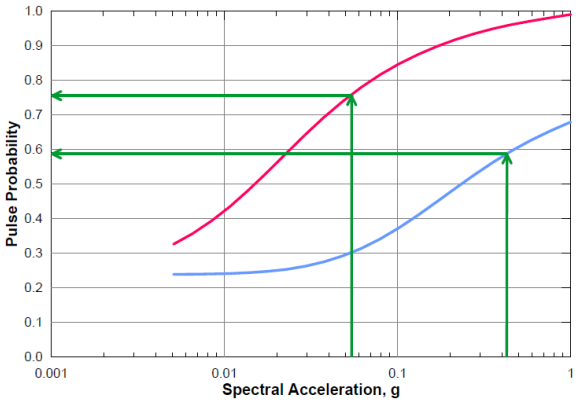

Fig. 5 – Pulse probability for T=0.75 sec (blue) and 7.0 sec (red) at bedrock

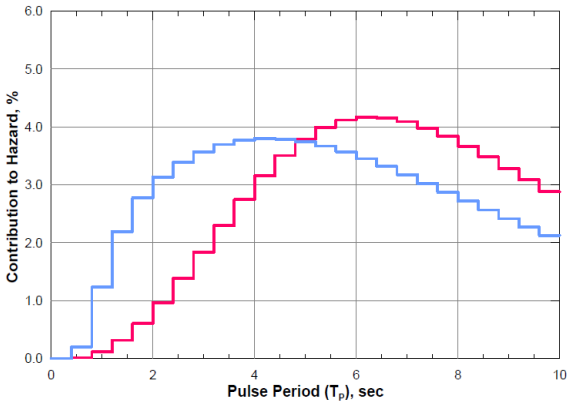

Fig. 6 – Hazard deaggregation in terms of pulse period for T=0.75 sec (blue) and 7.0 sec (red)

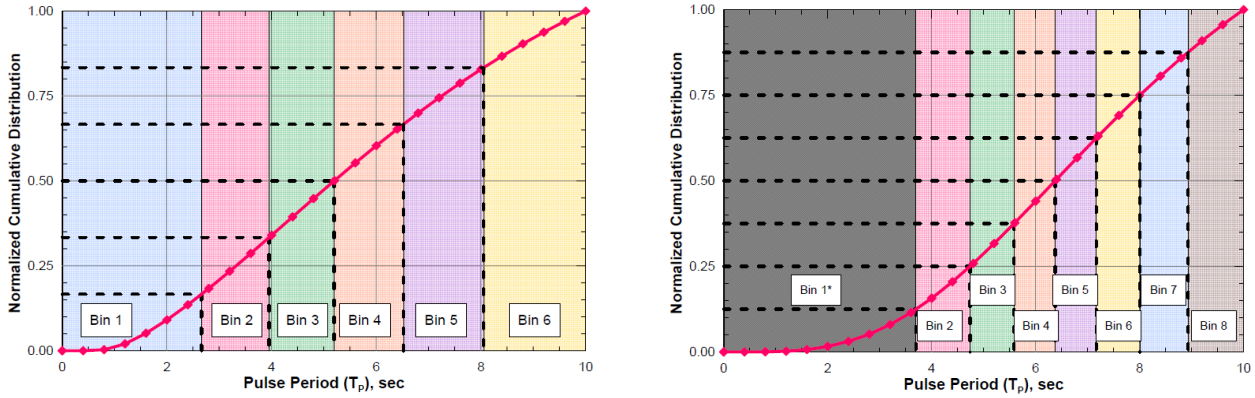

Fig. 7 – Normalized cumulative hazard distribution for T=0.75 sec (left) and 7.0 sec (right); Bin1 for the long period suite was discarded due to reasons listed in Section 4.3

4.4 Target bedrock response spectra

4.4.1 Pulselike motions: pulse-included CMS

The target bedrock response spectra for pulselike motions was based on pulse-included CMS, with a unique CMS for each of the T_p bins described in Section 4.3. The pulse-included CMS were constructed using the baseline deterministic scenario (M_w 8.0 event on the San Andreas; R = 14.7 km) and applying the pulse amplification relationship per [15] for each target T_p bin selected above. The additional epsilon term on the

pulse amplification equation was scaled for each pulse-included CMS such that the response spectral acceleration at the conditioning period matched that of the MCE_R at the corresponding period. The resulting CMS for pulselike motions for T = 0.75 sec and T = 7.0 sec are shown in Fig. 8.

4.4.2 Non-pulselike motions: conventional CMS

The target bedrock response spectra for non-pulselike motions are based on the conventional CMS spectra (see Fig. 3). For both the short period and long period suites, the maximum demand and RotD50 CMS were used to define the major and minor axis target spectra used in the bidirectional spectral matching, presented later in Section 5.2.2 of this paper.

4.4.3 Envelope of CMS

Per Section 16.2.1.2 of ASCE 7-16, the envelope of the maximum demand spectra of the two suites were required to not fall below 75% of the code-defined MCE_R spectrum over the period range of interest. This check was performed after the spectral matching procedure and presented in Section 5.3 of this paper.

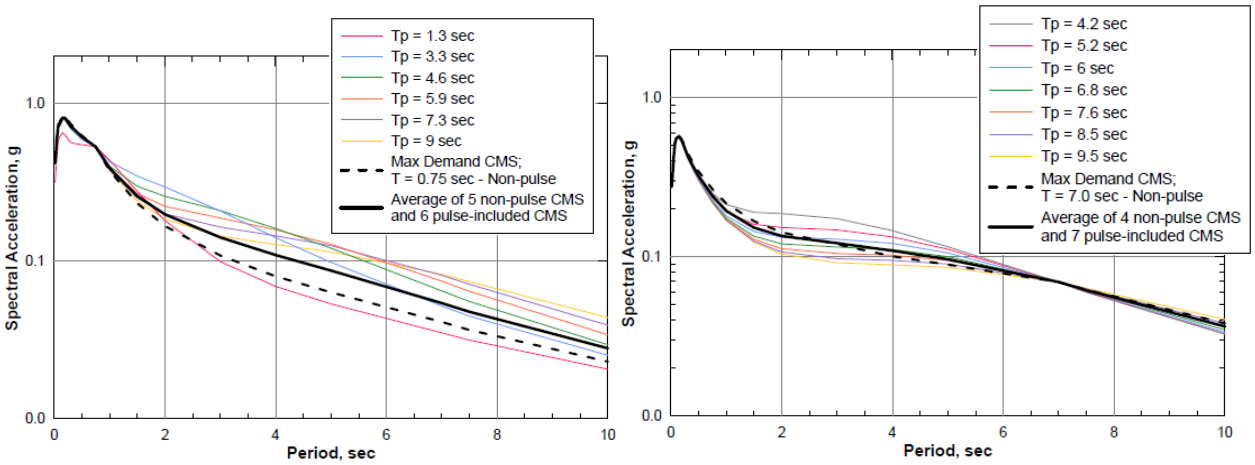

Fig. 8 – Pulse-included CMS and non-pulse max demand CMS for T=0.75 sec (left) and 7.0 sec (right)

5. Development of Bedrock Ground Motion Time Histories

5.1 Seed selection

The hazard deaggregation results were used to select appropriate seed ground motion records. Table 2 lists the seed motion records selected for the long period suite while those for the short period suite is omitted in the interest of space. The search tool available from the NGA-West2 database [17] for seed records based on several criteria summarized below:

- Tectonic setting and fault type – given that the seismic hazard at the site is governed by the shallow crustal events from the San Andreas fault, only shallow crustal events were selected;
- Spectral shape – the response spectrum of seed motions comparable to the target response spectrum is important to preserve the original waveform characteristics through spectral matching;
- Duration – a median significant duration ($D_{5\text{-}95}$; [18]) of about 33 sec was desired based on estimates from an empirical model [e.g., 19, 20];
- Earthquake magnitude, M_W – M_w of 8.0 is the controlling magnitude. The selected seeds range from M_w of 6.5 to M_w of 8.0;
- Site-to-source distance, R – the controlling R is approximately 15 km. This criterion was relaxed to allow for R_{rup} values up to 75 km; and
- Site condition, V_{S30} – the V_{S30} at the site is approximately 1,200 m/s. It was attempted to select records with similar site conditions, but Site Class B records are limited. The spectral matching procedure

modifies the frequency content to match the target, hence this criterion was relaxed to allow for Site Class C records.

- Pulse period (T_P) – for the pulselike motions, seed candidates were evaluated based on the recorded pulse period being comparable to the target T_P bins (Fig. 7).

Table 2 - Seed records for long period at bedrock (T = 7.0 sec)

No	T_p Range		Year	Earthquake	M_w	Fault Type	Station	Record Sequence No. (RSN)	Closest Distance (km)	V_{S30} (m/sec)
1*	3.70	4.74	1979	Imperial Valley-06	6.5	Strike slip	El Centro Array #6	181	1.4	203
2*	4.74	5.58	1999	Chi-Chi, Taiwan	7.6	Reverse Oblique	TCU075	1510	0.9	573
3*	5.58	6.37	1999	Kocaeli, Turkey	7.5	Strike slip	Gebze	1161	10.9	792
4*	6.37	7.17	1978	Tabas, Iran	7.4	Reverse	Tabas	143	2.1	767
5*	7.17	8.00	1999	Chi-Chi, Taiwan	7.6	Reverse Oblique	TCU046	1486	16.7	466
6*	8.00	8.93	2010	Darfield, New Zealand	7	Strike slip	DSLC	6897	8.5	296
7*	8.93	10.00	1992	Landers	7.3	Strike slip	Barstow	838	34.9	370
8	N.A.		1999	Kocaeli, Turkey	7.5	Strike slip	Istanbul	1164	52.0	595
9	N.A.		1999	Chi-Chi, Taiwan	7.6	Reverse Oblique	TTN051	1594	36.7	665
10	N.A.		1999	Hector Mine	7.1	Strike slip	Cabazon	1773	77.0	377
11	N.A.		2010	El Mayor-Cucapah, Mexico	7.2	Strike slip	Anza Borrego	5842	58.0	585

*pulselike motions

5.2 Spectral matching analysis

This section describes the modification of the selected seed records to match the appropriate target spectra via time-domain spectral matching. For pulselike motions, only the pulse-included component was spectrally matched while the orthogonal component was linearly scaled. The bedrock motions developed herein (both orthogonal horizontal components) had to be scaled up by 10% in order to have the fault parallel response spectra meet the Tall Buildings Initiative (TBI; [21]) criterion.

5.2.1 Pulselike motions

The seed motions were rotated to the orientation of the maximum spectral displacement at the respective conditioning period, while also checking that the pulselike characteristics are preserved. The rotated seed motions were then linearly scaled, typically to match the spectral acceleration at the conditioning period of their corresponding pulse-included CMS target. The amplitude-scaled pulse-included component of the seed motion was then spectrally matched to its associated pulse-included CMS target using the time-domain spectral matching computer program, RspMatch09 [22]. The minimum demand component is defined as orthogonal to the maximum demand component. Each of the individual minimum demand components was linearly scaled using the same scale factor as its maximum demand counterpart. Where necessary, this scale factor was adjusted to maintain a ratio of the two horizontal components similar to that of the as-recorded seed motion pair. This ensured that the direction of the maximum response is maintained for the global seismic response history analysis.

Baker [23] developed a quantitative method to identify pulselike motions via a Pulse Indicator score and determine the period of the extracted velocity pulse using the wavelet decomposition. The Pulse Indicator ranges between 0 and 1, with its value close to 1 showing a strong indication of being pulselike. Baker [23] considered motions with Pulse Indicator above 0.85 as pulselike motions. The extracted pulse period (T_P) along with the corresponding Pulse Indicator [23] are checked before and after spectral matching. An example of the rock motion time histories and response spectra of the spectrally-matched pulselike motions for the long period suite is shown in Fig. 9.

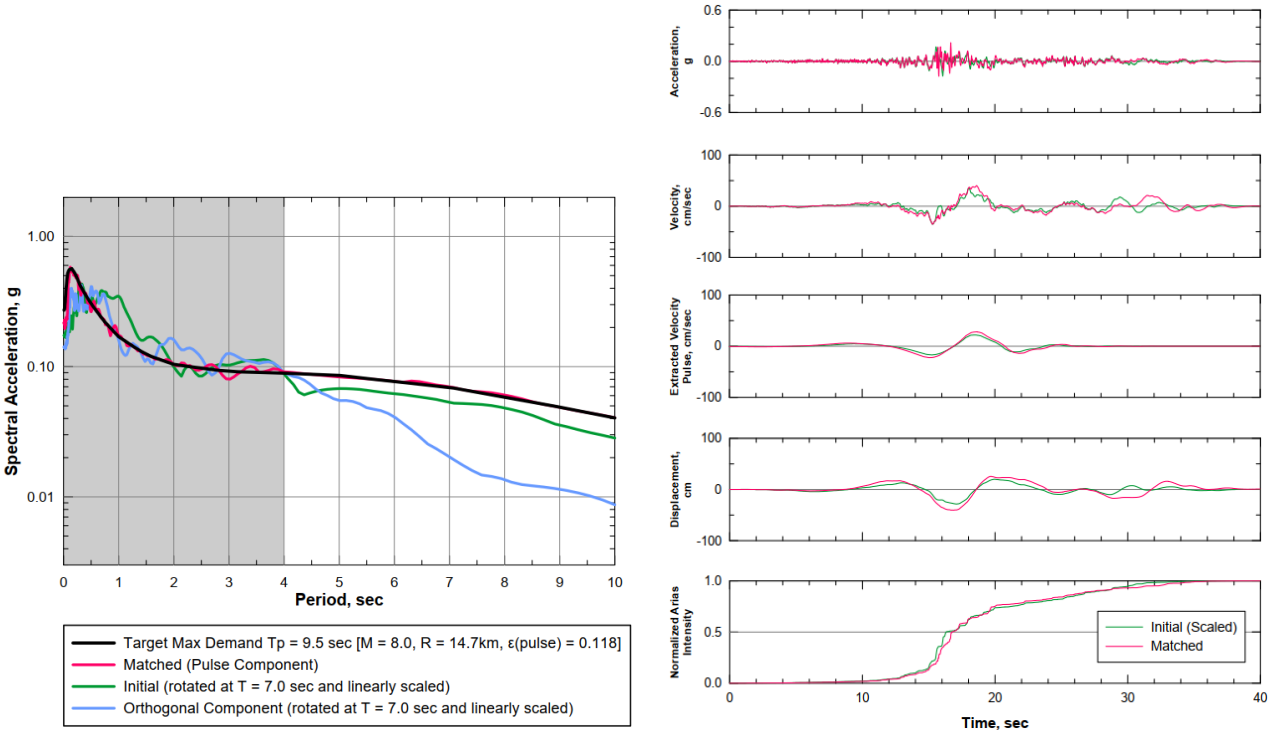

Fig. 9 – An example of spectrally-matched pulselike motions for long period suite (T=7.0 sec): RSN838 - 1992 Landerrs (BRS)

5.2.2 Non-pulselike motions

Typically, the maximum demand spectrum is used as a target spectrum for matching a single component of a seed motion while the other component is matched separately to a minimum demand target spectrum (often conservatively defined by geomean or RotD50). This procedure incorrectly implies that the maximum demand response will occur in the same orientation for all periods (Stewart et al., 2011) and, more importantly, this matching process leads to considerable overestimation of the maximum demand response in orientations other than those in which the two components are applied. On the basis of this observation, Grant (2011) developed a program, RSPMatchBi for matching the major and minor axis spectra of two horizontal ground-motion components simultaneously to two target spectra. Each pair of non-pulselike motions was adjusted using RSPMatchBi such that over all orientations, each "pair" of the matched horizontal motions has its maximum and minimum spectral accelerations matching the target maximum demand and RotD50 spectra, respectively. Examples of spectrally-matched non-pulselike motions are omitted herein due to space limitations.

5.3 Envelope of average short and long period spectra

The average max demand spectra of the matched motions for the short and long period suites are shown in Fig. 10. Also, the envelope of the average response spectra for the matched short and long period suites is shown in Fig. 11, which demonstrates compliance to Section 16.2.1.2 of ASCE 7-16, with the envelope of the CMS not falling below 75% of the MCE_R in the period range of interest (0.4 to 10 sec).

5.4 Orientation of Ground Motions

In accordance with Section 16.2.4 of ASCE 7-16 for near-fault sites, each pair of horizontal ground motion components was rotated to the fault-normal (FN) and fault-parallel (FP) directions of the governing causative fault, the San Andreas fault. The rotated motions were used in subsequent site response and SSI analyses.

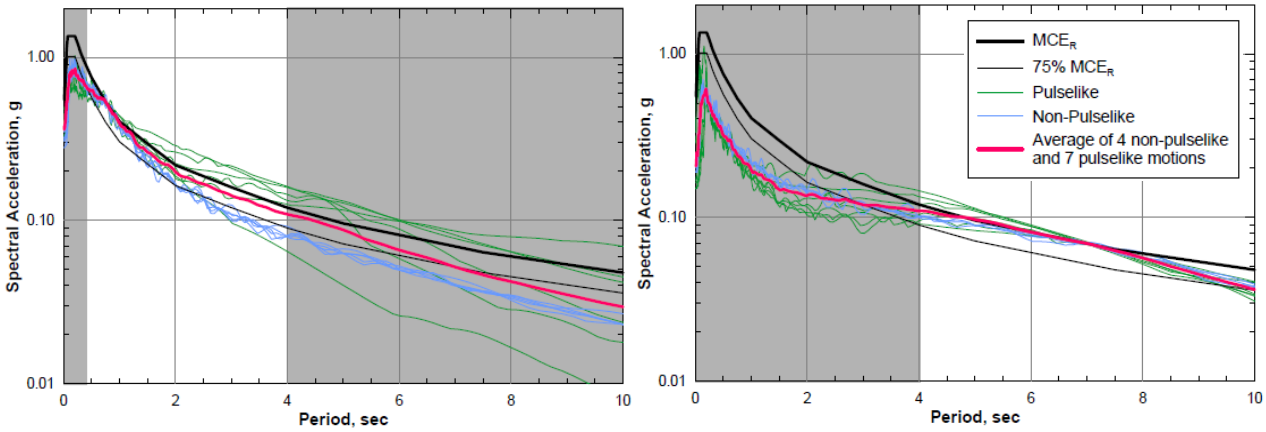

Fig. 10 – Average max demand spectra of matched motions for the short (left) and long (right) period suites

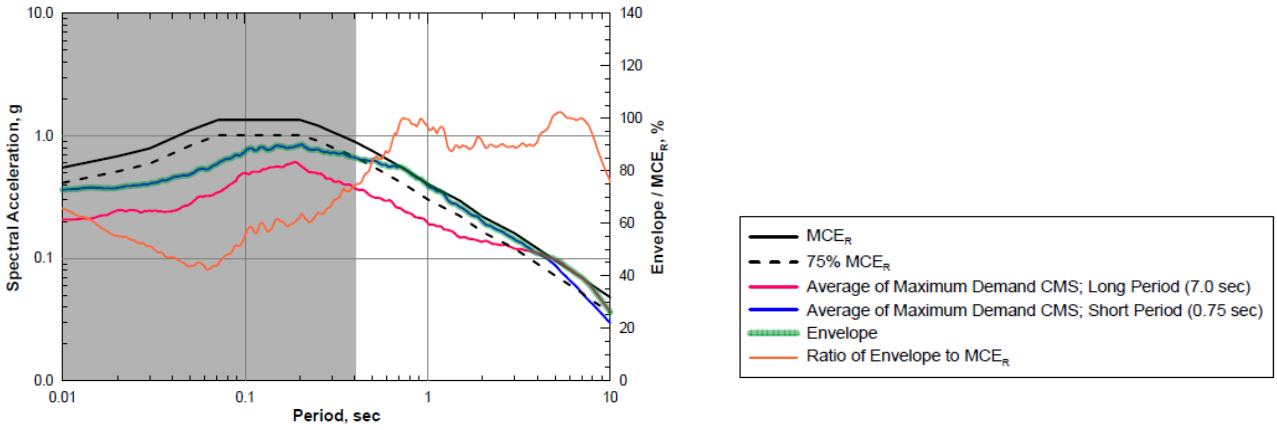

Fig. 11 – Envelope of matched short and long period average max demand spectra compared to the code-defined MCE$_R$ at bedrock

6. Conclusion

A case history of developing design ground motions for a high-rise in downtown San Francisco was presented, which incorporated directivity effects (velocity pulses). In addition to conventional PSHA, "pulse-included" PSHA was carried out to account for near-fault effects and evaluate the site-specific characteristics of near-fault pulselike ground motions and their hazards. Based on the PSHA results, two suites of near-fault ground motions were developed in accordance with the design standard, ASCE 7-16, including pulselike motions. This methodology has been successfully used on past high-profile projects in San Francisco including the Salesforce, 181 Fremont, and Park Towers for nonlinear response history analyses such as seismic site response analysis and soil-structure-interaction analysis, subjected to rigorous peer review.

7. Acknowledgements

We would like to thank the peer review panel: Shah Vahdani, Ron Hamburger, and Greg Deierlein for the helpful comments and discussions to improve this work. Also, we thank Michael Valley for his valuable structural inputs.

8. References

[1] American Society of Civil Engineers (2017). Minimum Design Loads and Associated Criteria for Buildings and Other Structures, ASCE Standard.

[2] U.S. Geological Survey (2014). A Java library developed by USGS Earthquake Hazards Program (EHP) in support of the National Seismic Hazard Model Project (NSHMP); https://earthquake.usgs.gov/.

[3] Petersen, M. D., Moschetti, M. P., Powers, P. M., Mueller, C. S., Haller, K. M., Frankel, A. D., Zeng, Yuehua, Rezaeian, Sanaz, Harmsen, S. C., Boyd, O. S., Field, N., Chen, R., Rukstales, K. S., Luco, Nico, Wheeler, R. L., Williams, R. A., and Olsen, A. H. (2014). Documentation for the 2014 update of the United States national seismic hazard maps: U.S. Geological Survey Open-File Report 2014–1091, 243 p.

[4] Field, E. H., Arrowsmith, R., Biasi, G. P., Bird, P., Dawson, T. E., Felzer, K. R., Zeng, Y. (2014). Uniform California Earthquake Rupture Forecast, version 3 (UCERF3) -The time-independent model. Bulletin of the Seismological Society of America, 104(3), 1122-1180. https://doi.org/10.1785/0120130164

[5] Boore, D. M., Stewart, J. P., Seyhan, E., and Atkinson, G. M. (2014). NGA-West 2 Equations for Predicting PGA, PGV, and 5%-Damped PSA for Shallow Crustal Earthquakes. Earthquake Spectra, 30 (3), 1057-1085.

[6] Campbell, K. W. and Bozorgnia, Y. (2014). NGA-West2 Ground Motion Model for the Average Horizontal Components of PGA, PGV, and 5%-Damped Linear Acceleration Response Spectra. Earthquake Spectra, 30 (3), 1087-1115.

[7] Chiou, B. S.-J. and Youngs, R. R. (2014). Update of the Chiou and Youngs NGA Model for the Average Horizontal Component of Peak Ground Motion and Response Spectra. Earthquake Spectra, 30 (3), 1117-1153.

[8] Abrahamson, N., Silva, W., and Kamai, R. (2014). Summary of the ASK14 Ground Motion Relation for Active Crustal Regions. Earthquake Spectra, 30 (3), 1025-1055.

[9] Boore, D. M. (2010). Orientation-Independent, Nongeometric-Mean Measures of Seismic Intensity from Two Horizontal Components of Motion. Short Note, Bulletin of the Seismological Society of America, 100 (4), pp. 1830-1835.

[10] Shahi, S. and Baker, J. W. (2013). NGA-West2 Models for Ground-Motion Directionality. PEER Report 2013/10, May.

[11] Baker, J. W. and Cornell, C. A. (2006). Spectral shape, epsilon and record selection. Earthquake Engng Struct. Dyn. 2006; 35:1077–1095.

[12] Baker, J. W. and Jayaram, N. (2008). Correlation of Spectral Acceleration Values from NGA Ground Motion Models. Earthquake Spectra, 24 (1), 299–317.

[13] Almufti, I., Motamed, R., Grant, D.M., and Willford, M. (2015). Incorporation of velocity pulses in design ground motions for response history analysis using a probabilistic framework. Earthquake Spectra: August 2015, Vol. 31, No. 3, pp. 1647-1666.

[14] Shahi, S., and Baker, J. W. (2011). An empirically calibrated framework for including the effects of near-fault directivity in probabilistic seismic hazard analysis. Bulletin of the Seismological Society of America, 101(2), 742–755.

[15] Shahi, S. (2012). A Probabilistic Framework to include the Effects of Near-Fault Directivity in Seismic Risk Assessment. Ph.D. Dissertation. Department of Civil and Environmental Engineering, Stanford University, November.

[16] Oasys (2018). Sismic 9.6 Manual, Probabilistic Seismic Hazard Program, Version 9.6 Build 16 by Arup.

[17] Pacific Earthquake Engineering Research Center (PEER) (2016). New NGA-West2 Ground Motion Database.

[18] Trifunac, M. D., and Brady, A. G. (1975). Study on duration of strong earthquake ground motion. Bulletin of the Seismological Society of America, 65(3), 581-626.

[19] Kempton, J. J. and Stewart, J. P. (2006). Prediction Equations for Significant Duration of Earthquake Ground Motions Considering Site and Near-Source Effects. Earthquake Spectra, 22 (4), 985–1013.

[20] Lee, J. (2015). Strong Ground Motion Durations of Directivity Motions. Proceeding of 6th International Conference on Earthquake Geotechnical Engineering, Christchurch, New Zealand, November 1 – 4.

[21] Pacific Earthquake Engineering Research Center (PEER) (2017). Guidelines for Performance-Based Seismic Design of Tall Buildings, Version 2.03. PEER Report No. 2017/06.

[22] Al Atik, L. and Abrahamson, N. (2010). An improved method for nonstationary spectral matching. Earthquake Spectra, Vol. 26 (3), pp. 601–617.

[23] Baker, J. W. (2007). Quantitative Classification of Near-Fault Ground Motions using Wavelet Analysis. Bulletin of the Seismological Society of America, 97 (5), 1486–1501.

